

The coherent scattering function of the reptation model: Simulations compared to theory

A. Baumgärtner¹, U. Ebert², and L. Schäfer^{3,a}

¹ Institut für Festkörperforschung, Forschungszentrum Jülich, 52425 Jülich, Germany

² Centrum voor Wiskunde en Informatica, P.O. Box 94079, 1090 GB Amsterdam, The Netherlands

³ Universität Essen, Universitätsstr. 5, 45117 Essen, Germany

Received 4 April 2003 and Received in final form 9 July 2003 /

Published online: 11 November 2003 – © EDP Sciences / Società Italiana di Fisica / Springer-Verlag 2003

Abstract. We present results of Monte Carlo simulations measuring the coherent structure function of a chain moving through an ordered lattice of fixed topological obstacles. Our computer experiments use chains up to 320 beads and cover a large range of wave vectors and a time range exceeding the reptation time. For additional information we also measured the coherent structure function of internal pieces of the chain. We compare our results i) to the predictions of the primitive chain model, ii) to an approximate form resulting from Rouse motion in a coiled tube, and iii) to our recent evaluation of the full reptation model. i) The primitive chain model can fit the data for times $t \gtrsim 20T_2$, where T_2 is the Rouse time of the chain. Besides some phenomenological amplitude factor this fit involves the reptation time T_3 as a second fit parameter. For the chain lengths measured, the asymptotic behavior $T_3 \sim N^3$ is not attained. ii) The model of Rouse motion in a tube, which we have criticized before on theoretical grounds, is shown to fail also on the purely phenomenological level. iii) Our evaluation of the full reptation model yields an excellent fit to the data for both total chains and internal pieces and for all wave vectors and all times, provided specific micro-structure effects of the MC dynamics are negligible. Such micro-structure effects show up for wave vectors of the order of the inverse segment size and enforce the introduction of some phenomenological, wave-vector-dependent prefactor. For the dynamics of the total chain our data analysis based on the full reptation model shows the importance of tube length fluctuations. Universal (Rouse-type) internal relaxation, however, is unimportant. It can be observed only in the form of the diffusive motion of a short central subchain in the tube. Finally, we present a fit formula which in a large range of wave vectors and chain lengths reproduces the numerical results of our theory for the scattering from the total chain.

PACS. 83.10.Kn Reptation and tube theories – 82.35.Lr Physical properties of polymers – 83.10.Rs Computer simulation of molecular and particle dynamics

1 Introduction

Dynamical properties of dense polymer systems like melts or dense solutions are often analyzed within the framework of the reptation model [1, 2]. Reptation is a specific mechanism for the motion of a single tagged chain through an environment of other chains. It is based on the idea that the background chains act as impenetrable obstacles which confine the motion of the tagged chain to a tube roughly defined by its present configuration. The local motion of the inner parts of the chain is restricted to the diffusion of little wiggles of “spared length” along the tube. Globally the motion is driven by the chain ends, where wiggles are created or destroyed. Creation of a wiggle shortens the tube by its spared length, destruction prolongs the tube

in some randomly chosen direction. In the long run this motion of the chain ends leads to the complete destruction of the original tube and to large scale diffusion of the chain.

Formulated in more precise terms, the reptation model deals with the stochastic motion of a flexible chain embedded in a fixed environment of obstacles which form the edges of a regular lattice in three-dimensional space. In this work we present results for the coherent structure function measured in an extensive simulation of this model. The measured coherent structure functions of the total chain and of internal subchains are compared to the results of our recent analytical evaluation [3] of the model. For the total chain there exist previous approximate theories based on reptation [4, 5], which are included in the comparison. These theories do not treat the full

^a e-mail: lsphy@Theo-Phys.Uni-Essen.DE

dynamics of the model, but neglect so-called “tube length fluctuations”. For typical chain lengths used in (computer or physical) experiments these fluctuations are known to yield important contributions, as has first been pointed out in reference [6] in the context of an analysis of the viscosity.

As mentioned above, results of the reptation model are generally used to analyze data for systems like polymer melts [7], where the surrounding of a given chain certainly is far from forming an ordered time-independent lattice of obstacles. Clearly the surrounding chains slowly move away, which leads to “constraint release” [8], an effect that becomes important [7] outside the limit of asymptotically long chains. Also disorder in the distribution of obstacles might lead to fluctuations in the local tube diameter, thus affecting the local mobility of spared length. In this work we omit all such effects of the environment and study the coherent structure function of the pure reptation model, as described above. This is a necessary prerequisite for an analysis aiming at the separation of the different effects present in a real melt.

To illustrate the problem we now briefly recall some typical results [1,2] of reptation, as established for very long chains. We concentrate on the motion of an internal segment, which from a theoretical point of view is the simplest quantity to discuss.

Simple as it is, the reptation scenario involves several time scales and leads to a rich phenomenology. It needs a microscopic time T_0 before the chain feels the existence of constraints due to its surrounding. Generally, T_0 is taken as the Rouse time of a short subchain of N_e segments: $T_0 \sim N_e^2$, where the “entanglement length” N_e is chosen such that the coil diameter of the subchain is of the order of the diameter of the tube, which substitutes the surrounding chains. The second time scale T_2 is the relaxation time of the total chain in a fixed tube, *i.e.* the time a wiggle needs to diffuse over the whole chain. It depends on chain length N as $T_2 \sim T_0(N/N_e)^2 \sim N^2$ and thus behaves as the relaxation time of a free chain in the Rouse model. The longest scale T_3 is the “reptation time”. It measures the time which the motion of the chain ends needs to completely destroy the initial tube. In the limit of long chains the reptation model predicts [1] $T_3 \sim (N/N_e)^3 T_0$.

For observables like the motion of individual segments the model yields asymptotic power laws, where the exponent depends on the time range. We quote here the results for the motion of the central segment $j = N/2$:

$$\left\langle \overline{(\mathbf{r}_{N/2}(t) - \mathbf{r}_{N/2}(0))^2} \right\rangle \sim \begin{cases} t^{1/4} & ; T_0 \ll t \ll T_2, \\ (t/N)^{1/2} & ; T_2 \ll t \ll T_3, \\ t/N^2 & ; T_3 \ll t, \end{cases} \quad (1.1)$$

We use the bar to denote the dynamic average, *i.e.* the average over the motion of spared length. The pointed brackets stand for the average over all initial configurations.

Considerable effort has been invested to check these predictions in simulations of melts, but the outcome to date is not conclusive [7,9,10]. The $t^{1/2}$ -regime has never been properly identified. (Note that crossover from a re-

gion $\langle \overline{(\mathbf{r}_j(t) - \mathbf{r}_j(0))^2} \rangle \sim t^\alpha$, $\alpha < \frac{1}{2}$, to free diffusion easily can pretend the existence of a $t^{1/2}$ -regime. What has to be demonstrated is the stability of this regime for a larger range of time and chain lengths.) Slowing-down of segment motion in the range $T_0 < t < T_2$ is observed [9] with an effective exponent somewhere between 1/4 and 1/2. Only for some related observable, measuring the motion of a central segment relative to the center of mass, a $t^{1/4}$ -behavior seems to be established [10]. Real experiments do not measure $\langle \overline{(\mathbf{r}_j(t) - \mathbf{r}_j(0))^2} \rangle$. However, a related quantity, the return-to-origin probability of a segment averaged over all segments, is measured in NMR experiments. Here the equivalent to $t^{1/4}$ -behavior has been found in reference [11], but reference [12] reports equivalent results only for motion through a crosslinked gel, where constraint release is suppressed. The corresponding melt shows a quite different behavior.

Invoking tube length fluctuations and constraint release, we may qualitatively interpret the observed deviations from the asymptotic reptation results as crossover behavior outside the region of asymptotic chain lengths. However, there exist other theories of melt dynamics, which are not based on the tube concept and describe many experiments as well [13,14]. (See also the review [7].) Thus it is conceivable that the basic assumptions of the reptation scenario do not hold. To get more insight into these problems, we clearly have to quantitatively evaluate the consequences of the pure reptation model, beyond asymptotic power laws.

In previous analytical work [15,16] we determined the motion of individual segments of the chain. Since our theory involves some approximations, we compared the results to simulations [17] of the Evans-Edwards model [18], which is an accurate implementation of the pure reptation model. In essence, both theory and simulations agreed in showing that the crossover among various asymptotic power law regions is very slow. The crossover regions are so broad that the asymptotic power laws can be identified only for very long chains. For example, using the Evans-Edwards model with the smallest possible tube diameter we could identify the $t^{1/4}$ -law for the motion of the central segment only for chain lengths $N \gtrsim 160$. This law is the easiest to observe, and our evaluation of the theory predicts that other asymptotic laws unambiguously can be identified only for much longer chains. This result is in line with the known slow crossover behavior of the reptation time [6], which is predicted to reach the asymptotic law $T_3 \sim N^3$ only for chain lengths far beyond present day experimental feasibilities. Still, for the motion of individual segments, the full crossover functions can be calculated, and our analytical results very well agree with our simulations. Furthermore, for shorter chains all our analytical and simulational results qualitatively are very similar to results of simulations of melts [9,10]. In a later work [19] we considered chain motion in a time independent, but disordered environment, where the disorder affects only the chain mobility but leaves the equilibrium distribution of chain configurations unchanged. We found that with such “kinematic” disorder reptation prevails,

an observation which recently has been supported [20] by rigorous bounds on the diffusion coefficient. Since such kinematic disorder certainly is present in a melt, these results again support reptation as adequate theory of melt dynamics.

In contrast to the motion of individual segments the coherent structure function $S_c(q, t; N)$, ($q = |\mathbf{q}|$: scattering vector, t : time), is well accessible in real experiments. It can be measured, for instance, by neutron scattering from a mixture of deuterated and hydrogenated chains. As mentioned above, approximate asymptotic forms for $S_c(q, t; N)$, based on reptation-type theories, can be found in the literature [4,5]. However, as for the motion of individual segments we can evaluate the full reptation theory for $S_c(q, t; N)$ also outside the asymptotic regime. As for individual segments, we then expect to see important preasymptotic or crossover effects. The evaluation of $S_c(q, t; N)$ including full reptational dynamics is somewhat complicated, and our theory in detail has been presented in reference [3]. Here we compare the results to simulations of the Evans-Edwards model. We consider both the scattering from the total chain and from interior subchains. The latter is important to estimate the reliability of the theory, which can treat end-effects only in some approximation.

In Section 2 we discuss our simulations. Section 3 is devoted to a comparison with the expressions for $S_c(q, t; N)$ given by Doi and Edwards [4,2] or by de Gennes [5], respectively. In Section 4 we qualitatively describe our theory and give an empirical fit formula which describes our quantitative results reasonably well. The comparison between our theory and our Monte Carlo data is presented in Section 5. Section 6 contains our conclusions.

2 Simulations

2.1 The Evans-Edwards model

A very simple model for simulating reptation has been introduced by Evans and Edwards [18]. The configuration $\{\mathbf{r}_1, \dots, \mathbf{r}_N\}$ of the chain is taken as a random walk of $N - 1$ steps $|\mathbf{r}_j - \mathbf{r}_{j-1}| = \ell_0$ on a cubic lattice. The lattice spacing ℓ_0 henceforth defines the unit of length. The obstacles are taken as the edges of the dual lattice. In the interior of the chain, the obstacles suppress any motion except for the motion of “hairpins”, *i.e.*, configurations of three subsequent beads of type $\{\mathbf{r}_{j-1}, \mathbf{r}_j, \mathbf{r}_{j+1} = \mathbf{r}_{j-1}\}$. In an elementary move the tip \mathbf{r}_j of the hairpin with equal probability hops to any of the six neighbors of the site $\mathbf{r}_{j-1} = \mathbf{r}_{j+1}$. The chain ends $\mathbf{r}_1, \mathbf{r}_N$ are free to hop between all neighbors of $\mathbf{r}_2, \mathbf{r}_{N-1}$, respectively. Figure 1 shows a sequence of internal configurations resulting from this dynamics. In our simulations we used the same implementation of the model as in our previous work [17], and we measured the coherent structure function defined

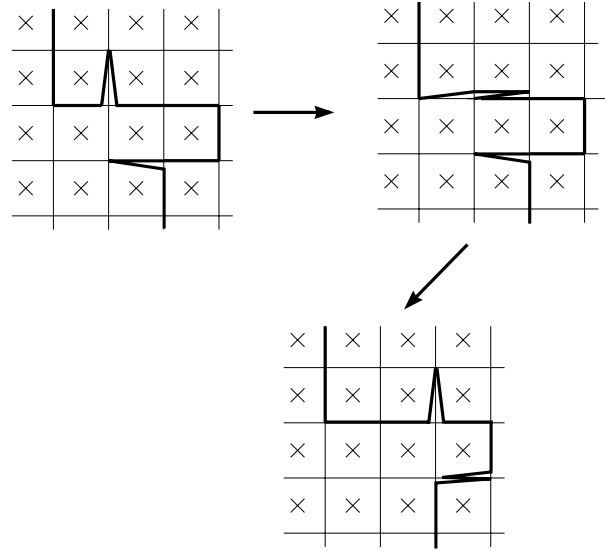


Fig. 1. A series of subsequent chain configurations illustrating the microscopic dynamics of the Evans-Edwards model (in its two-dimensional version). The crosses represent impenetrable obstacles.

as

$$S_c(q, t^{(\text{MC})}; N) = \sum_{j_1, j_2=1}^N \left\langle e^{i\mathbf{q}(\mathbf{r}_{j_1}(t^{(\text{MC})}) - \mathbf{r}_{j_2}^{(0)})} \right\rangle = \overline{\langle \mathcal{C}(\mathbf{q}, t^{(\text{MC})}) \mathcal{C}(\mathbf{q}, 0) + \mathcal{S}(\mathbf{q}, t^{(\text{MC})}) \mathcal{S}(\mathbf{q}, 0) \rangle}, \quad (2.1)$$

where

$$\mathcal{C}(\mathbf{q}, t) = \sum_{j=1}^N \cos(\mathbf{q}\mathbf{r}_j(t)),$$

$$\mathcal{S}(\mathbf{q}, t) = \sum_{j=1}^N \sin(\mathbf{q}\mathbf{r}_j(t)). \quad (2.2)$$

(The imaginary part $\mathcal{S}(\mathbf{q}, t)\mathcal{C}(\mathbf{q}, 0) - \mathcal{C}(\mathbf{q}, t)\mathcal{S}(\mathbf{q}, 0)$ of S_c is zero on average, of course.) To get more information on the internal motion, we also measured the coherent structure function $S_c(q, t^{(\text{MC})}; M, N)$ of the central subchain of length M , defined by restricting the summations in equations (2.1, 2.2) to the interval $[(N - M)/2 + 1, (N + M)/2]$. From our previous work, we expect to see features characteristic of reptation for $N \gtrsim 100$, and we therefore used chain lengths $N = 80, 160, 320$. Since for our model, the entanglement length is estimated as $N_e \approx 3.7$ (see Sect. 4.2), this yields values $22 \lesssim N/N_e \lesssim 87$. Similar values are extracted from many simulations or experiments on melts, so that our results should be relevant also for the interpretation of such data. Monte Carlo time $t^{(\text{MC})}$ is measured in units of one attempted move per bead on average. We performed runs up to $t_{\text{max}}^{(\text{MC})} = 5 \cdot 10^{10}$, and we measured the structure function up to $t^{(\text{MC})} = 4.5 \cdot 10^9$ using a moving time average.

2.2 Statistical accuracy

During a run, the longer chains do not diffuse very far, and data of a single run therefore are strongly correlated. To get reasonably accurate results we have to average over many independent runs. *A priori*, this poses a problem for larger momenta, $qR_g \gtrsim 1$, where R_g is the radius of gyration of the chain. It is easily checked that the reduced width of the distribution of the static structure function with increasing qR_g rapidly tends to 1. Indeed, in the limit $N \rightarrow \infty, q > 0$ fixed, the distribution of $S_c(q, 0; N)$ approaches the exponential distribution. This suggests that 10^4 runs are needed to reduce the statistical uncertainty to a few percent. This would pose no problems, if we just were interested in static properties. However, for the longer chains a single run extending to times well beyond the reptation time takes several hours on a standard work station. In measuring *dynamic* quantities the number of runs therefore inevitably is much smaller than needed for a precise determination of *static* quantities.

Fortunately it turns out that the dynamics essentially is decoupled from the static configuration. This is illustrated in Figure 2, which shows results for $S_c(q, t^{(\text{MC})}; N), ql_0 = 0.5, N = 320$, normalized to the exact static structure function $S_0(q, N)$ of the model, which easily is calculated analytically (see Sect. 2.4). Each curve in Figure 2a is averaged over 10^3 independent short runs ($t^{(\text{MC})} \leq 10^5$), including the moving time average for each run. Clearly, the scatter of $S_c(q, 0; N)$ is consistent with the above discussion. It is larger than the temporal variation of the curves. However, plotting in Figure 2b the normalized time dependence $[S_c(q, t^{(\text{MC})}; N) - S_c(q, 0; N)]/S_0(q, N)$, we find that all curves nearly coincide. The global dynamics measured by the structure function, is not correlated with the static configuration, an observation which supports one of the basic assumptions of the reptation model. The reason behind that observation is easily understood. The mobility of the chain is governed by the number of hairpins which essentially is Gaussian distributed and fluctuates much less than the static structure function. Furthermore, except for rare events, *viz.* extremely stretched or extremely compact configurations, the number of hairpins is independent of the overall (tube) conformation of the chain. With this insight, we take as basic data the difference $S_c(q, t^{(\text{MC})}; N) - S_c(q, 0; N)$ for each run. The error bars in our plots give twice the standard deviation of this difference. We always plot the normalized dynamic structure function defined as

$$\begin{aligned} \bar{S}_c(q, t^{(\text{MC})}; N) = 1 + \frac{1}{S_0(q, N)} \\ \cdot \left(S_c(q, t^{(\text{MC})}; N) - S_c(q, 0; N) \right)_{\text{averaged over runs}} \end{aligned} \quad (2.3)$$

where $S_0(q, N)$ is the exact static structure function, not the measured average value of $S_c(q, 0; N)$. Depending on the number of independent runs, these two quantities differ by 0.1–6%.

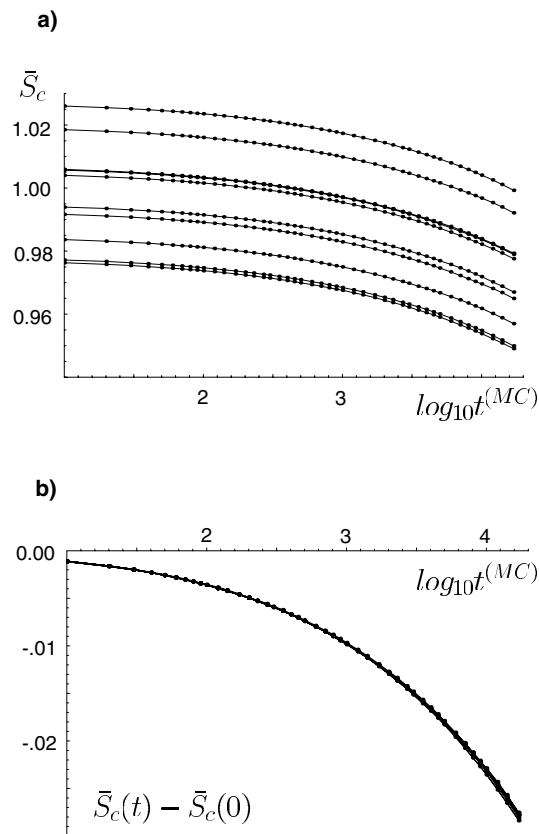


Fig. 2. Data for the coherent structure function ($N = 320, q = 0.5$) as a function of $\log_{10} t^{(\text{MC})}$ in the short-time regime. $\bar{S}_c(q, t^{(\text{MC})}; N)$ is normalized to the exact static structure function $S_0(q, N)$ (Eq. (2.6)). a) Ten sets of data, each averaged over 10^3 independent runs. The lines serve to guide the eye. b) The same sets of data as in a), but with $\bar{S}_c(q, 0; N)$ subtracted.

For reasons of computer memory, we performed runs with three different values of the maximal time $t_{\text{max}}^{(\text{MC})}$. To observe the small initial effects, for each value of chain length N and wave vector $|\mathbf{q}|$, we averaged over 10^4 short runs with $t_{\text{max}}^{(\text{MC})} = 10^5$, taking data up to $t^{(\text{MC})} = 1.4 \cdot 10^4$. These data are denoted by small dots in the following figures. In the intermediate time range, $t_{\text{max}}^{(\text{MC})} = 10^8$, we measured the structure function for $10^4 \leq t^{(\text{MC})} \leq 10^7$ and always performed 50 runs (heavy dots in the figures). In the long time range, $t_{\text{max}}^{(\text{MC})} = 5 \cdot 10^{10}$, we took data for $10^5 \leq t^{(\text{MC})} \leq 4.5 \cdot 10^9$, averaging over 30 to 100 runs (circles in the figures). For each set of runs with given maximal time, we also measured the average of $S_c(q, 0; N)$.

For additional information on the statistical accuracy of our data, we measured the imaginary part of $S_c(q, t^{(\text{MC})}; N)$, which rigorously vanishes for $t^{(\text{MC})} = 0$, but fluctuates about zero for $t^{(\text{MC})} > 0$ in a finite sample. For longer times we typically found average values of order $\pm 0.01 S_0(q, N)$, again smaller than the uncertainty of $S_c(q, 0; N)$ in long-time runs.

2.3 Momentum range

First considerations suggest to restrict the analysis to the momentum range $R_g^{-2} \ll q^2 \ll \ell_0^{-2}$. Momenta of order $q^2 R_g^2 \lesssim 1$ do not resolve the tube but rather see a cloud of beads. For momenta $q^2 \ell_0^2 \gtrsim 1$ the micro-structure of the chain might play a role. In our simulations the above condition can only poorly be satisfied. For our longest chain ($N = 320$) it reads $0.02 \ll q^2 \ell_0^2 \ll 1$, leaving at best a small window close to $q \ell_0 \approx 0.4$.

However, a closer inspection reveals that these considerations do not seriously restrict dynamic measurements. To check the relevance of the condition $q^2 \ell_0^2 \ll 1$, we analyzed the dynamics of a free chain. As is well known, asymptotically the standard Rouse dynamics is found if for a lattice chain “kink jumps”: $\{\mathbf{r}_j - \mathbf{r}_{j-1} = \mathbf{s}_1, \mathbf{r}_{j+1} - \mathbf{r}_j = \mathbf{s}_2\} \Rightarrow \{\mathbf{r}_j - \mathbf{r}_{j-1} = \mathbf{s}_2, \mathbf{r}_{j+1} - \mathbf{r}_j = \mathbf{s}_1\}$, $\mathbf{s}_1 \cdot \mathbf{s}_2 = 0$ are allowed besides hairpin moves. We found that with this modified dynamics, the normalized coherent structure function is in excellent agreement with the relaxation function calculated from the continuous chain Rouse model, even for $q \ell_0 = 1$. Micro-structure effects arising from the finite segment size die out very rapidly on the scale of about 10 MC steps and therefore should be negligible also for reptation dynamics. Of course this does not exclude the possibility of dynamical micro-structure effects which might influence the short-time regime and are not accounted for by the reptation model. In particular, reptation does not properly treat the dynamics of fluctuations perpendicular to the tube axis.

Concerning the condition $q^2 R_g^2 \gg 1$, we note that smaller wave vectors, of course, provide little information on the details of the internal motion of the chain, but at least they measure the global motion of the coil. However, the slowness of this motion asks for extremely large time ranges $t_{\max}^{(\text{MC})} \gg T_3$. We, therefore, performed only one series of simulations for $|\mathbf{q}| \ell_0 = 0.1$, $N = 160$, corresponding to $q^2 R_g^2 = 0.267$. Most of our simulations use values $3 \lesssim q^2 R_g^2 \lesssim 50$, with a maximal value of $q^2 R_g^2 \approx 53$ reached for $|\mathbf{q}| \ell_0 = 1$, $N = 320$.

2.4 Normalization

In our simulations we choose \mathbf{q} to point into one of the three lattice directions. For that choice, the static correlations between segments j and k take the form

$$\begin{aligned} \left\langle e^{i\mathbf{q}(\mathbf{r}_j(0) - \mathbf{r}_k(0))} \right\rangle &= \left(\frac{2}{3} + \frac{1}{3} \cos |\mathbf{q}| \right)^{|k-j|} \\ &= \exp(-\bar{q}^2 |k-j|), \end{aligned} \quad (2.4)$$

where

$$\bar{q}^2 = -\ln \left(\frac{2}{3} + \frac{1}{3} \cos |\mathbf{q}| \right). \quad (2.5)$$

Recall that the lattice constant ℓ_0 defines the unit of length. Summing the segment indices over the chain, we

find the static structure function which is used in normalizing our results:

$$\begin{aligned} S_0(q, N) &= \sum_{j,k=1}^N \exp(-\bar{q}^2 |k-j|) \\ &= N + \frac{2}{(e^{\bar{q}^2} - 1)^2} \left[e^{-\bar{q}^2(N-1)} - N + (N-1) e^{\bar{q}^2} \right]. \end{aligned} \quad (2.6)$$

In our simulations, we, for each run, averaged over all three lattice directions.

3 Comparison of data and simplified reptation-type theories

3.1 Asymptotic form of $S_c(\mathbf{q}, t; \mathbf{N})$ derived by Doi and Edwards

A simplified version of the reptation model concentrates on the dynamics of the “primitive chain” [2, 4], which is a reduced form of the chain, lying stretched in the tube. In the Evans-Edwards model the primitive chain can be viewed as the non-reversal random walk derived from the random walk configuration of the physical chain by cutting off all hairpins. All internal degrees of freedom are neglected so that within the time interval Δt , all parts of the primitive chain move the same distance Δs along the tube. The length of the primitive chain is taken to be fixed. (This model is often addressed as “the reptation model”). We will use the term “primitive chain model” to distinguish it from the full reptation model which deals with the dynamics of spared length as the elementary process.)

With its simplifications, the primitive chain model treats only the destruction of the initial tube, as resulting from the global motion of the chain. It neglects tube length fluctuations which are due to the uncorrelated motion of the chain ends as well as relaxation in the interior of the tube. Since both these additional effects are governed by the equilibration time T_2 of the chain, the primitive chain model is restricted to times $t \gg T_2$. Furthermore, the segment indices are taken as continuous variables, and this “continuous chain limit” restricts the theory to long chains: $N \gg 1$.

Within this model the time-dependent correlation function of two beads,

$$S(q, t; j, k, N) = \left\langle \overline{\exp[i\mathbf{q}(\mathbf{r}_j(t) - \mathbf{r}_k(0))]} \right\rangle, \quad (3.1)$$

obeys a diffusion equation. Solving this equation and integrating j, k over the chain, Doi and Edwards arrive at the following result for the normalized coherent structure function (see Ref. [2], Chapt. 6.3.):

$$\bar{S}_c(q, t; N) = \frac{S_c(q, t; N)}{S_c(q, 0; N)} = \bar{S}_{\text{DE}}(q^2 R_g^2, t/T_3), \quad (3.2)$$

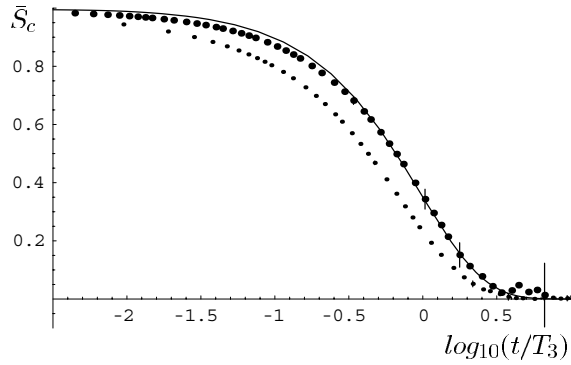


Fig. 3. \bar{S}_c measured for $q^2 R_g^2 \approx 3.3$ as a function of t/T_3 in the long-time regime. Heavy dots: $N = 320$; small dots: $N = 80$. Full curve: primitive chain result (3.3). $T_3(N = 320)$ has been adjusted to bring the long-time tail of the data for $N = 320$ on top of the theoretical curve. $T_3(80) = T_3(320)/4^3$. Some typical error bars (two standard deviations) are shown for $N = 320$. The statistical error rapidly decreases with decreasing t/T_3 . For $t/T_3 < 10^{-0.5}$ it is smaller than the size of the dots.

$$\bar{S}_{\text{DE}}(Q, \tau) = \frac{1}{D(Q)} \sum_{p=1}^{\infty} \frac{Q \sin^2 \alpha_p}{\alpha_p^2 (Q^2/4 + Q/2 + \alpha_p^2)} \exp(-\alpha_p^2 \tau). \quad (3.3)$$

Here the α_p are the positive solutions of

$$\alpha_p \tan \alpha_p = \frac{1}{2} Q = \frac{1}{2} q^2 R_g^2, \quad (3.4)$$

and

$$D(Q) = \frac{2}{Q^2} (e^{-Q} - 1 + Q) \quad (3.5)$$

is the Debye function. With the assumptions of the theory, the reptation time attains its asymptotic behavior $T_3 \sim N^3$. Note that T_3 is related to the time scale τ_d introduced in reference [2] by $T_3 = \frac{\pi^2}{4} \tau_d$.

The result (3.2, 3.3) for $\bar{S}_c(q, t; N)$ depends only on $Q = q^2 R_g^2 \sim \bar{q}^2 N$ and $\tau = t/T_3 \sim t/N^3$, but not on N separately. To test this feature, we carried through simulations for $N = 320, q = 0.25$ and $N = 80, q = 0.5024$, both parameter sets resulting in $q^2 R_g^2 \approx 3.3$. Figure 3 compares our simulation results to \bar{S}_{DE} , plotted as a function of $\log_{10}(t/T_3)$. The Monte Carlo time has been scaled so that in the region $t/T_3 \gtrsim 1$, the data for $N = 320$ fit to the theoretical curve. In view of $T_3 \sim N^3$, for $N = 80$ an additional factor 4^3 has been included in the time scale. With this scaling, the deviation between the two sets of data shown in Figure 3 proves that we have not yet reached chain lengths large enough for the primitive chain model to hold.

Still, for larger times, \bar{S}_{DE} and the data for $N = 320$ agree quite well. This suggests to treat $T_3 = T_3(N)$ as a fit parameter in adjusting the data to $\bar{S}_{\text{DE}}(q^2 R_g^2, t/T_3)$, giving up the strict proportionality $T_3 \sim N^3$. However, a closer inspection of Figure 3 reveals that the data initially decrease faster than \bar{S}_{DE} . This is a systematic effect, observed for all chain lengths and wave vectors. It

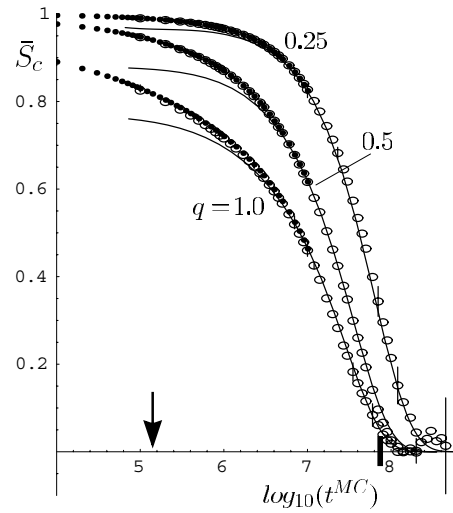


Fig. 4. Data for $\bar{S}_c(q, t, N)$ for chain length $N = 320$, wave vectors $|\mathbf{q}| = 0.25, 0.5, 1.0$, as a function of the Monte Carlo time; dots: medium-time runs ($t_{\text{max}}^{\text{MC}} = 10^8$); circles: long-time runs ($t_{\text{max}}^{\text{MC}} = 4.5 \cdot 10^9$). The curves give the results of the primitive chain model, fitted to the data as explained in the text. The arrow points to the equilibration time $T_2^{\text{MC}}(320)$, the heavy bar gives $T_3^{\text{MC}}(320) = 10^{7.82}$. Some typical error bars (two standard deviations) are shown for $q = 1.0, 0.25$.

points to the influence of relaxation modes neglected in the primitive chain model. According to a suggestion of de Gennes [5], internal relaxation, in particular, yields an initial decrease of $\bar{S}_c(q, t; N)$ which saturates at some q -dependent plateau value. We thus should fit the data to $B_{\text{DE}} \bar{S}_{\text{DE}}(q^2 R_g^2, t/T_3)$, with B_{DE} as another free parameter.

A detailed analysis of the reptation model points to tube length fluctuations as the origin of the initial decrease, rather than internal relaxation. (See Sect. 4.3 and Ref. [3].) Still we may fit our data to $B_{\text{DE}} \bar{S}_{\text{DE}}$, where $B_{\text{DE}} = B_{\text{DE}}(q, N)$, $T_3 = T_3(N)$. Figure 4 shows the results for $N = 320$. We clearly find a very good agreement between theory and data in the time region $t \gtrsim 20T_2$. (The estimate for T_2 has been taken from our theory, see Sect. 4.2.) Deviations occur for smaller times, which is consistent with the approximations inherent in the primitive chain model. Within the realm of that model the central segment moves according to $\langle (r_{N/2}(t) - r_{N/2}(0))^2 \rangle \sim (t/N)^{1/2}$, $T_2 \ll t \ll T_3$ (cf. Eq. (1.1)), and from our previous work [17] we know that this law certainly is not attained before $t \gtrsim 20T_2$. The results shown in Figure 4 are typical also for other chain lengths.

Since T_3 now plays the role of an effective fit parameter, it *a priori* could depend both on N and q . Parameters $T_3 = T_3(q, N)$, $B_{\text{DE}} = B_{\text{DE}}(q, N)$ extracted by fitting our data are collected in Table 1. Any q -dependence of T_3 is found to be weak, if significant at all. B_{DE} depends on q , but is essentially independent of N .

Table 1. Parameter values for the fit of $B_{\text{DE}}\bar{S}_{\text{DE}}(q^2 R_g^2, t/T_3)$ to the data. Reptation time $T_3^{(\text{MC})}$ is measured in Monte Carlo steps.

$N^{(\text{MC})}$	q	$\log_{10} T_3^{(\text{MC})}(q, N)$	$B_{\text{DE}}(q, N)$
80	0.5024	5.90	0.91
160	0.10	6.91	0.997
	0.50	6.87	0.89
	1.00	6.82	0.76
320	0.25	7.85	0.965
	0.50	7.82	0.88
	1.00	7.80	0.78

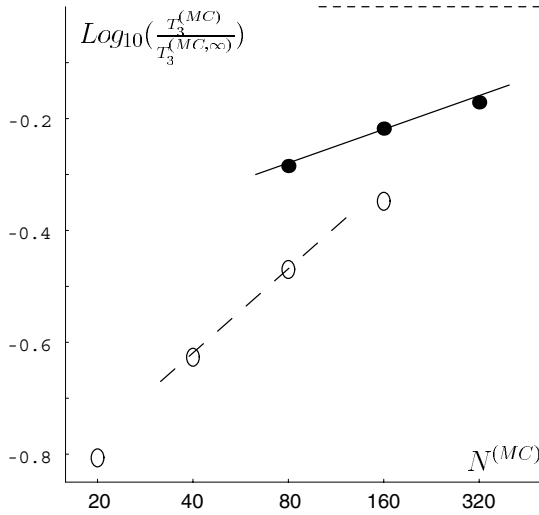


Fig. 5. Results for the reptation time defined in terms of the long-time behavior of \bar{S}_c (dots) or in terms of the motion of the end segment (circles). The asymptotic behavior $T_3 \sim N^3$ has been divided out. The lines correspond to power laws $T_3 \sim N^{3.2}$ (full line) or $T_3 \sim N^{3.5}$ (broken line). The short-dashed line gives the asymptotic limit.

Ignoring any q -dependence, in Figure 5 we have plotted the values of $T_3(N)$ normalized to the asymptotic behavior T_3^∞ resulting from equations (4.5, 4.7, 4.12) below. It must be stressed that here we *define* a reptation time in terms of the large-time behavior of the scattering function (and the Doi-Edwards form \bar{S}_{DE}). Other definitions based on other observables (or other theoretical expressions) may yield somewhat different results. In previous work [17], we defined a reptation time \tilde{T}_3 by the criterion that the mean-squared distance moved by a chain end equals the equilibrium mean-squared end-to-end distance: $\langle (\mathbf{r}_0(\tilde{T}_3) - \mathbf{r}_0(0))^2 \rangle = R_e^2$. The previous data are included in Figure 5 (open circles). The two definitions yield somewhat different results for the corrections to the asymptotic behavior. In the range of N measured here, \tilde{T}_3 is about 30% below T_3 as taken from the scattering function. It, however, must be noted that the values extracted from the scattering functions depend somewhat on

the time range included in the fit. We estimate this uncertainty to be of the order of 5%. In Figure 5 we included lines corresponding to effective power laws $T_3 \sim N^z$. The effective powers are consistent with expectations based on previous work [6].

To summarize, our results show that the coherent structure function of the primitive chain model may well be used to fit data for large times, $t \gtrsim 20T_2$, provided we allow for some phenomenological prefactor B_{DE} and take the reptation time T_3 as an effective parameter defined by the fit. For smaller times, deviations are seen, that increase with increasing q .

3.2 Comparison to the Gennes' theory

In his work [5], de Gennes considers only intermediate values of q : $\ell_0^{-2} \gg q^2 \gg R_g^{-2}$ and constructs the scattering function as a sum of two terms. For $t \gg T_2$ the ‘‘creep’’ term dominates. This term is just the limiting form of \bar{S}_{DE} (Eq. (3.3)) for $Q \rightarrow \infty$:

$$\bar{S}^{(c)}(t, N) = \frac{8}{\pi^2} \sum_{p=0}^{\infty} (2p+1)^{-2} \exp \left[-(2p+1)^2 \frac{\pi^2}{4} \frac{t}{T_3} \right]. \quad (3.6)$$

It tends to 1 for $t/T_3 \rightarrow 0$. It is combined with some contribution of local relaxation, which is calculated in two steps. First, the interior relaxation of a Rouse chain in one-dimensional space is calculated, where the chain is stretched so that the end-to-end distance equals the tube length. In the second step this one-dimensional motion is embedded into the three-dimensional random walk configuration of the tube. Tube length fluctuations are neglected. With some additional approximation, this model of a Rouse chain in a coiled tube yields a ‘‘local’’ contribution

$$\bar{S}^{(\ell)}(q, t) = e^{t_1} \operatorname{erfc} \sqrt{t_1}, \quad (3.7)$$

where

$$t_1 = \frac{3}{4} \frac{N}{N_e} (q^2 R_g^2)^2 \frac{t}{T_3}. \quad (3.8)$$

Since again the validity of the asymptotic law $T_3 \sim N^3/N_e$ is assumed, the chain length N and the entanglement length N_e drop out in equation (3.8), as expected for a contribution resulting from strict one-dimensional internal relaxation. $\bar{S}^{(\ell)}(q, t)$ describes internal relaxation on length and time scales exclusively determined by q . The total result for the normalized coherent scattering function reads

$$\bar{S}_c(q, t; N) = \bar{S}_{\text{dG}}(q, t; N) = (1 - B_{\text{dG}}) \bar{S}^{(\ell)}(q, t) + B_{\text{dG}} \bar{S}^{(c)}(t, N), \quad (3.9)$$

where, according to de Gennes,

$$B_{\text{dG}} = B_{\text{dG}}(q) = 1 - \frac{N_e}{36} q^2 \ell_0^2 \quad (3.10)$$

is independent of N .

In an attempt to extend the range of wave vectors to $q\ell_0 \gtrsim 1$, Schleger *et al.* [21] used $B_{dG}(q) = \exp(-q^2\ell_0^2 N_e/36)$. With this choice it was found [21–23] that $\bar{S}_{dG}(q, t; N)$ over a large range of wave vectors and for several chain lengths yields a good fit to neutron scattering data from melts of polyethylene. However, Pütz *et al.* [10], using the same form of $\bar{S}_{dG}(q, t; N)$ to analyze simulation data for melts of very long chains, found only poor agreement. In later work [24] they argued that this was due to some ambiguity in the relation between entanglement length N_e and tube diameter.

In our recent work [3] we reconsidered the model of a Rouse chain in a tube. Our analysis reveals some serious deficiency of this model: it does not start from equilibrium initial conditions. An ensemble of stretched one-dimensional random walk chains folded into the three-dimensional random walk configuration of the tube is not identical to the equilibrium ensemble of three-dimensional random walk chains. The local structure of the chains differs on the scale of the tube diameter. For the static structure function, this yields a correction of relative order N_e/N that vanishes in the limit $q^2 R_g^2 = \text{const}$, $N \rightarrow \infty$. For the time dependence, however, the effect is serious since the non-equilibrium initial conditions relax only on scale T_2 . Our analysis shows that this unphysical relaxation indeed dominates the time dependence of the “local” contribution $\bar{S}^{(\ell)}(q, t)$, as calculated from this model (see Fig. 3 of Ref. [3]). Data analysis based on equation (3.9) with $\bar{S}^{(\ell)}(q, t)$ taken from the model of a Rouse chain in a tube, therefore, is not particularly meaningful.

Still, in view of the experimental findings cited above, we may ask whether equations (3.6–3.9) can be used as heuristic modeling of the coherent structure function resulting from reptation. Figure 6 shows the result for the longest chain ($N = 320$) and largest wave vector ($q = 1.0$) measured. The resulting value $q^2 R_g^2 \approx 53.3$ is large enough for a reasonable test of the form (3.9), which assumes $q^2 R_g^2 \gg 1$. Replacing in equation (3.9) \bar{S}_c by the full result \bar{S}_{DE} of the primitive chain model does not seriously change the picture. The reptation time is fixed by the long-time tail and is taken from Table 1. For B_{dG} , we used the form suggested by Schleger *et al.*: $B_{dG} = \exp(-q^2\ell_0^2 N_e/36)$. N_e in principle is known from our previous analysis of segment motion: $N_e = 3.69$ (see Sect. 4.2). Thus, all parameters are fixed and the result for \bar{S}_{dG} (full curve in Fig. 6) strongly deviates from the data, except for the extreme long-time tail. This is no surprise since the value $B_{dG} \approx 0.9$, resulting for $N_e = 3.69$, considerably exceeds the value $B_{DE} \approx 0.78$ extracted from fitting with the Doi-Edwards form. (See Tab. 1.) If we treat B_{dG} as a free parameter, we clearly in the range $t \gtrsim 20T_2$ can enforce agreement among theory and data, (see Fig. 4), at the expense of considerably underestimating \bar{S}_c for $t \lesssim T_2$. The situation can be improved only, if we also change the scale of t_1 , dividing t_1 , (Eq. (3.8)), by a factor of order 200. Quite similar results are found for $N = 160$, where t_1 has to be divided by a factor of order 50 to reproduce the average trend of the data for $t \lesssim T_2$.

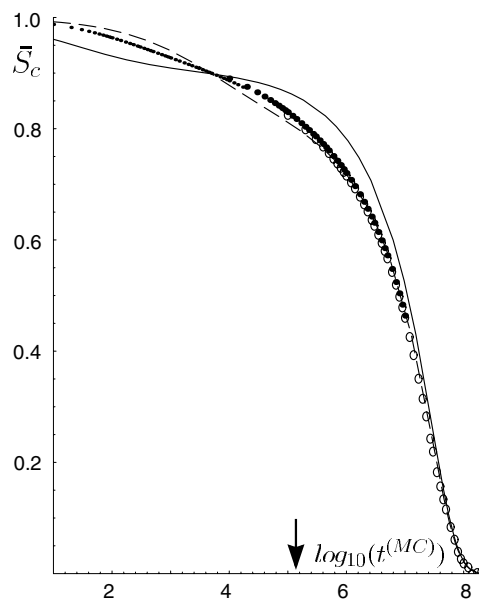


Fig. 6. Fit of \bar{S}_{dG} (Eq. (3.9)) to data for $N = 320$, $q = 1.0$. Solid line: $N_e = 3.69$, corresponding to $B_{dG} = 0.903$; dashes: $B_{dG} = 0.82$, t_1 (Eq. (3.8)) divided by 200. The arrow points to the equilibration time $T_2^{(MC)}$. Data, small dots: short-time runs ($t_{\max}^{(MC)} = 10^5$); heavy dots: medium-time runs ($t_{\max}^{(MC)} = 10^8$), circles: long-time runs ($t_{\max}^{(MC)} = 5 \cdot 10^{10}$).

We conclude that also from a purely phenomenological point of view, the form (3.9) of \bar{S}_c is not justified. The large and chain-length-dependent rescaling required for t_1 suggests that tube length fluctuations governed by the time scale T_2 might be much more important than internal relaxation processes governed by an N -independent scale.

We finally note that in reference [23] a modified form of equation (3.9) has been proposed, in which the creep term $\bar{S}^{(c)}$ is calculated from tube length fluctuations, but the form (3.7) of the local contribution is retained. The analysis is restricted to the time range $t \ll T_2$, which is the relevant range for neutron scattering experiments. From Figure 6 it is clear that with the proper parameter values $N_e = 3.69$, t_1 as given in equation (3.8), this modification cannot improve the fit for $t \ll T_2$, since tube length fluctuations only decrease the contribution $\bar{S}^{(c)}$. Again a reasonable fit can be reached only if we take both B_{dG} and the scale of t_1 as free parameters.

4 Results of the full reptation model

4.1 Basic ideas of our approach

The primitive chain model neglects all internal degrees of freedom, and an attempt to model internal relaxation as one-dimensional Rouse motion leads to unphysical initial conditions, which seriously affect the results up to times of the order of the internal relaxation time T_2 . However, the simplifying assumptions underlying these approaches

are not an essential part of the original reptation model. As recalled in the introduction, reptation as single elementary process involves the diffusion of spared length along the chain, together with its decay and creation at the chain ends. The separation of the dynamics into internal relaxation, tube length fluctuations and motion of the primitive chain therefore is somewhat artificial. In particular, tube length fluctuations cannot properly be separated from the motion of the primitive chain, as will be discussed in Section 4.3. Furthermore, from our analysis of segment motion we know that for typical experimental chain lengths we are in a crossover region where all dynamic effects must be treated on the same level by evaluating the consequences of full reptational dynamics.

In our analytical work [16,3] we use a very simple implementation of the reptation idea, in which the wiggles of spared length are represented by particles which hop along the chain, with hopping probability p per time step. The particles do not interact, and a given particle sees the others just as part of the chain. If a particle passes a bead, it shifts the position of this bead in the tube by the spared length ℓ_S . The chain ends are coupled to large particle reservoirs, which absorb and emit particles at such a rate that the equilibrium density ρ_0 of spared length on the chain is maintained on the average. Absorption or emission of a particle prolongs or shortens the tube at the corresponding chain end by the spared length ℓ_S . Keeping track of the change in the occupation number of the reservoirs, we therefore control the tube length fluctuations as well as the destruction of the original tube. In particular, within time interval $[0, t]$ an end piece of length $\ell_S n_{\max}(t)$ of the original tube has been destroyed, where $n_{\max}(t)$ is the largest negative fluctuation of the occupation number of the corresponding reservoir during this time interval.

All moments of the stochastic processes which determine the motion of internal segments or the occupation of the reservoirs, can be evaluated rigorously, but the determination of the maximal fluctuation $n_{\max}(t)$ poses a serious problem. The occupation number of a reservoir carries out a *correlated* random process, since a particle emitted can be reabsorbed by the same reservoir later. This correlation dies out only on scale of the internal equilibrium time T_2 of the chain. It does not prevent the evaluation of arbitrary moments, but the maximal fluctuation cannot be calculated rigorously. Such a calculation is possible [25] only for an *uncorrelated* random process. To determine the degree of tube destruction, we therefore have to resort to some approximation. In our method, basically for each final time t we replace the correlated random process by that uncorrelated random walk which for this time yields the correct moments. The effective hopping rate of this random walk depends on the final time t . It changes from the microscopic rate $\rho_0 \cdot p$ for $t \ll T_2$ to the mobility $\rho_0 \cdot p/N$ of the primitive chain for $t \gg T_2$, which is a physically most reasonable behavior.

In essence, this “mean hopping rate” approximation for the coherent structure function smoothly interpolates between two rigorously accessible limits. For $t \ll T_2$, tube renewal does not influence the motion of an interior piece

of the chain, and the coherent structure function of such pieces can be calculated rigorously. For $t \gg T_2$ the correlations of the stochastic processes are negligible and the mean hopping rate approximation should become exact. Indeed, we find that in this limit the motion of all chain segments is tightly bound to the motion of the chain ends. As a result, the problem reduces to the uncorrelated motion of a single stochastic variable, as in the primitive chain model. The details of our approximation are discussed extensively in references [3,16], and will not be repeated here.

The coherent scattering function can be determined by summing the contribution of two beads

$$S(q, t; j, k, N) = \left\langle e^{i\mathbf{q}(\mathbf{r}_j(t) - \mathbf{r}_k(0))} \right\rangle \quad (4.1)$$

over the bead indices j, k . For this function, in reference [3], Section 6.1, we have derived an integral equation of the form

$$\begin{aligned} S(q, t; j, k, N) &= S^{(T)}(q, t; j, k, N) \\ &+ \int_0^t dt_0 \sum_{j_0=0}^N \left\{ \mathcal{P}^*(j_0, t_0|0) \exp(-\bar{q}^2|j_0 - k|) \right. \\ &\times S(q, t - t_0; j, 0, N) + \mathcal{P}^*(j_0, t_0|N) \exp(-\bar{q}^2|j_0 - k|) \\ &\left. \times S(q, t - t_0; j, N, N) \right\}. \end{aligned} \quad (4.2)$$

Here $dt_0 \mathcal{P}^*(j_0, t_0|m)$, $m = 0, N$, is the probability that the initial tube is finally destroyed within time interval $[t_0, t_0 + dt_0]$, its last piece being the initial position of segment j_0 , which at time t_0 is occupied by chain end 0 or N , respectively. The exponential factors result from the random walk configuration of the tube, cf. equations (2.4, 2.5). The inhomogeneity $S^{(T)}(q, t; j, k, N)$ is the contribution to $S(q, t; j, k, N)$ of all those stochastic processes, which do not completely destroy the original tube.

Summing equation (4.2) over the segments j, k we find a system of two equations which have to be solved numerically. The kernel \mathcal{P}^* and the inhomogeneity $S^{(T)}$ are determined within the mean hopping rate approximation. The results are lengthy and will not be reproduced here. In Section 4.4 we rather give an analytical expression, which in the range of wave vectors and chain lengths considered in the present work, reasonably well reproduces the numerical results of our theory.

We finally note that we analytically can prove (Ref. [3], Sect. 7) that our theory in the limit of infinite chain length $N \rightarrow \infty$, with t/T_3 and $q^2 R_g^2$ kept fixed, reproduces the result of the primitive chain model. Also the relation to the model of a Rouse chain in a tube can be analyzed in precise terms, if we consider an interior piece of length M in an infinitely long chain. We find (Ref. [3], Sect. 5) that this model reproduces the results of reptation only for $t/T_2(M) \rightarrow \infty$, $q^2 R_g^2(M)$ fixed, where $T_2(M)$ or $R_g(M)$ are the equilibration time and the radius of gyration of the subchain considered. For $t/T_2(M) \lesssim 1$ the non-equilibrium initial condition seriously affect the scattering function, as has been discussed in Section 3.2.

4.2 Microscopic parameters of the reptation model

The microscopic parameters of the model are the segment size $\ell_0 = |\mathbf{r}_j - \mathbf{r}_{j-1}|$, the average density ρ_0 of mobile particles on the chain, the spared length per particle ℓ_S , and the hopping rate p . Measuring all lengths in units of ℓ_0 , we introduce the dimensionless spared length

$$\bar{\ell}_S = \frac{\ell_S}{\ell_0}. \quad (4.3)$$

It turns out that for all times beyond truly microscopic times $t \lesssim 2/p$, the hopping rate p combines with t to yield the time variable

$$\hat{t} = pt, \quad (4.4)$$

which we will use in the sequel. The relation of \hat{t} to the Monte Carlo time $t^{(\text{MC})}$ introduces the fit parameter τ_0 :

$$\hat{t} = \tau_0 t^{(\text{MC})}. \quad (4.5)$$

Also ρ_0 and $\bar{\ell}_S$ combine into a single important parameter. The number of particles that passed over a bead on average increases with time, and if it is sufficiently large, the discreteness of the individual hopping processes becomes irrelevant. The results then depend only on the combination $\bar{\ell}_S^2 \rho_0$. In our previous work on the motion of individual segments [15–17], we found that $\bar{\ell}_S$ and ρ_0 separately enter the results only for $\hat{t} \lesssim 10^3$. In this time region, a segment on average has moved less than 10 steps in the tube and still feels the discreteness of the process. For the structure function we find that not even this small time region is seriously affected. If we ignore the discreteness of the hopping process, the results for all $\hat{t} > 1$ change by less than 0.5%, which coincides with the accuracy of our numerical evaluation. Thus the only microscopic parameters relevant for the coherent structure function are the combination $\bar{\ell}_S^2 \rho_0$ and the time scale τ_0 . The reason behind this empirically observed suppression of initial discreteness effects will be discussed in Section 4.3.

We, furthermore, note that also the discreteness of the underlying chain turns out to be unimportant. Provided we normalize the coherent structure function by the static structure function calculated for the same microstructure, for $N \gtrsim 50$ and wave vectors $q\ell_0 \lesssim 2$ within the above quoted accuracy we find the same results for a continuous chain as for the model where we sum over discrete bead indices j, k . This observation is consistent with the independence of statics and dynamics discussed in Section 2.2 and illustrates that our calculation indeed yields universal results.

Since in our simulations we use the same model as in our previous work on segment motion [17], we can take the numerical values of the microscopic parameters from there. In analyzing the Monte Carlo data, we thus use the value

$$\bar{\ell}_S^2 \rho_0 = 1.23. \quad (4.6)$$

Having a much larger set of data available than previously, we somewhat readjust the time scale. We use

$$\tau_0 = 6.8 \cdot 10^{-2}, \quad (4.7)$$

rather than the previous value $\tau_0 = 6.092 \cdot 10^{-2}$. For the logarithmic scale $\log_{10} \hat{t}$ of the figures in reference [17], this amounts to a shift by -0.048 , which does not change the good agreement among theory and experiment which in reference [17] is shown to hold over about 6 decades of time.

In our formulation of the reptation model, the entanglement length N_e , or the tube diameter $\ell_0 N_e^{1/2}$, equivalently, do not show up explicitly. They are hidden in the spared length and the density of the particles, *i.e.*, in the overall mobility of the chain. In contrast, the previous approaches explicitly involve these parameters. As discussed at the end of the last section, our theory in appropriate limits reproduces the previous results, which allows us [3] to relate our parameters $\bar{\ell}_S, \rho_0, p$ to those of these other models. Specifically, we find a relation for the entanglement length:

$$N_e = 3\bar{\ell}_S^2 \rho_0. \quad (4.8)$$

With the numerical value (4.6) this yields $N_e = 3.69$ and implies that for the Evans-Edwards model with the smallest possible obstacle spacing it needs about 4 steps before the obstacles come into play seriously.

We note that $\bar{\ell}_S \rho_0$ and thus N_e have been determined [17] by fitting data for the motion of individual segments in the time range $\hat{t} > 10^3$. N_e is thus not influenced by the deviations from the full reptation model occurring in the initial range $\hat{t} \lesssim 10^3$, as discussed below (Sect. 5). Thus, consistency of the analysis clearly enforces use of the same value N_e for all observables. We estimate the uncertainty of this value to be in the range of 5%.

We now also can give a quantitative definition of the time scales. Identifying the equilibration time T_2 with the Rouse time of a free chain of N segments, from the asymptotic relations among the models, we find

$$\hat{T}_2 = pT_2 = \frac{(N+1)^2}{\pi^2}. \quad (4.9)$$

The reptation time can be defined as the average lifetime of the original tube

$$\hat{T}_3 = p \int_0^\infty dt_0 t_0 \mathcal{P}^*(t_0). \quad (4.10)$$

Here $dt_0 \mathcal{P}^*(t_0)$ is the probability that the tube is finally destroyed within time interval $[t_0, t_0 + dt_0]$. It is related to the distribution $\mathcal{P}^*(j_0, t_0 | m)$ introduced in equation (4.2) via

$$\mathcal{P}^*(t_0) = \sum_{j_0=0}^N [\mathcal{P}^*(j_0, t_0 | 0) + \mathcal{P}^*(j_0, t_0 | N)]. \quad (4.11)$$

Evaluation in the asymptotic limit $N \rightarrow \infty$ yields

$$\hat{T}_3^{(\infty)} = \frac{N^3}{4\bar{\ell}_S^2 \rho_0} = \frac{3}{4} \frac{N^3}{N_e}. \quad (4.12)$$

In this limit, \hat{T}_3 is related to the reptation time τ_d introduced for the primitive chain model [2] as

$$\hat{T}_3^{(\infty)} = \frac{\pi^2}{4} p\tau_d, \quad (4.13)$$

which is the relation used in Section 3 in our analysis of the primitive chain model.

4.3 Qualitative discussion of the coherent structure function

Tube destruction, tube length fluctuations, and internal relaxation are different facets of the same microscopic dynamics. Therefore, any separation of these processes is to some extent artificial. Yet some rough discussion based on these concepts is useful with regard to the interpretation of the data presented in Section 5.

We first consider tube length fluctuations ΔL . Here a precise definition is possible by identifying ΔL with the fluctuations of the total spared length. On average the spared length equals $\ell_S \rho_0 N$, where $\rho_0 N$ is the average number of particles on the chain. Since the fluctuations of the particle number are essentially Gaussian distributed we find

$$\frac{\Delta L}{\ell_0} \approx \bar{\ell}_S \sqrt{\rho_0 N} = \sqrt{\frac{1}{3} N_e N}, \quad (4.14)$$

where N_e is introduced via equation (4.8). Within the equilibration time T_2 tube length fluctuations on average on both chain ends replace a piece of length $\Delta L/2$ of the original tube by a new piece. In real three-dimensional space, this new piece has an average extension of $\sqrt{\ell_0 \Delta L/2}$, and to observe the effect, the scattering vector must obey $q^2 \ell_0 \Delta L/2 \gtrsim 1$, or

$$q^2 \ell_0^2 \gtrsim \sqrt{\frac{12}{N_e N}}, \quad (4.15)$$

equivalently. For large wave vectors, the coherent structure function $S_c(q, t; N)$ is determined by the part of the original tube that still exists at time t . Taking only tube length fluctuations into account, we, therefore, find for $t \approx T_2$:

$$\begin{aligned} \bar{S}_c(q, T_2; N) &= \frac{S_c(q, t; N)}{S_c(q, 0; N)} \approx \frac{N - \Delta L/\ell_0}{N} \\ &\approx 1 - \sqrt{\frac{N_e}{3N}}, \end{aligned} \quad (4.16)$$

provided q is large compared to the bound (4.15). This estimate yields the effect of fully developed tube length fluctuations. With increasing chain lengths it is clearly suppressed, but it should be well visible up to fairly long chains $N/N_e \approx 10^2$.

Tube destruction in the sense of the primitive chain model is responsible for the main part of the decay of the coherent structure function. According to equation (4.16), it is the dominant effect as soon as $1 - \bar{S}_c(q, t; N) \gg \sqrt{N_e/3N}$. For $t \rightarrow T_2$, it is strongly correlated with tube length fluctuations which, seen from a microscopic point of view, drive the tube destruction. It, therefore, is no surprise that evaluating the coherent structure function of the primitive chain model, $\bar{S}_{\text{DE}}(q^2 R_g^2, t/T_3)$, for $q^2 R_g^2 \gg 1$

and time $t = T_2$, we find a decrease of the same order of magnitude as that due to tube length fluctuations:

$$\begin{aligned} 1 - \bar{S}_{\text{DE}}\left(q^2 R_g^2, \frac{T_2}{T_3}\right) &\stackrel{q^2 R_g^2 \gg 1}{\approx} 1 - \bar{S}^{(c)}(T_2, N) \\ &= \sqrt{\frac{2 T_2}{\pi T_3}} + O(e^{-\text{const } T_3/T_2}) \\ &\approx \sqrt{\frac{8}{3\pi^3} \frac{N_e}{N}} + O(e^{-\text{const } N}). \end{aligned} \quad (4.17)$$

Recall that $\bar{S}^{(c)}(t, N)$ (Eq. (3.6)) is the limit of \bar{S}_{DE} for $q^2 R_g^2 \gg 1$. Comparison of equations (4.16, 4.17) illustrates that tube length fluctuations cannot properly be separated from tube destruction. Being of the same order of magnitude for $t \approx T_2$, they strongly interfere in the full theory.

We finally note that the use of T_3 as fit parameter, necessary to fit the results of the primitive chain model to our data, illustrates that tube length fluctuations influence the efficiency of tube destruction for all times [6], even for chains of lengths $N/N_e \approx 100$.

Internal relaxation can be analyzed by considering a subchain of length M in the center of an infinitely long chain. We thus consider the coherent structure function

$$S_c(q, t; M, \infty) = \sum_{j,k=1}^M \left\langle e^{i\mathbf{q}(\mathbf{r}_j(t) - \mathbf{r}_k(0))} \right\rangle^\infty. \quad (4.18)$$

Within time t , segment j is displaced along the tube by $\bar{\ell}_s n$ steps, and since the tube has a random walk conformation, the average over the paths of segment j yields

$$\left\langle e^{i\mathbf{q}(\mathbf{r}_j(t) - \mathbf{r}_k(0))} \right\rangle^\infty = e^{-\bar{q}^2 |j + \bar{\ell}_s n - k|}.$$

This expression is to be averaged over the distribution $\mathcal{P}_1(n, t)$ of the number n of particles that diffused over bead j . We note that in the situation considered here $\mathcal{P}_1(n, t)$ is independent of j , since the process is translationally invariant along an infinitely long chain. We thus find

$$S_c(q, t; M, \infty) = \sum_{n=-\infty}^{+\infty} \mathcal{P}_1(n, t) \sum_{j,k=1}^M e^{-\bar{q}^2 |j + \bar{\ell}_s n - k|}. \quad (4.19)$$

Now shifting $j + \bar{\ell}_s n \rightarrow j$, we can rewrite this expression as

$$\begin{aligned} S_c(q, t; M, \infty) &= \sum_{n=-\infty}^{+\infty} \mathcal{P}_1(n, t) \left\{ \sum_{j,k=1}^M e^{-\bar{q}^2 |j - k|} \right. \\ &\quad \left. + \sum_{k=1}^M \left[\sum_{j=M+1}^{M+\bar{\ell}_s n} e^{-\bar{q}^2 |j - k|} - \sum_{j=1}^{\bar{\ell}_s n} e^{-\bar{q}^2 |j - k|} \right] \right\}. \end{aligned} \quad (4.20)$$

Since $\mathcal{P}_1(n, t)$ is normalized to 1, the first term in equation (4.20) yields the static structure function of the subchain. All time dependence results from the motion of the

end pieces of the subchain and thus is due to the length fluctuations and the shift of the subchain in the tube. Proper interior relaxation within the subchain has no effects on the coherent structure function.

We want to stress that this does *not* imply that our theory *neglects* interior relaxation. The basic relation (4.19) only exploits the fact that the segment j has carried out a random walk of $\bar{\ell}_s n$ steps. It does not imply that this walk is along the precise original configuration of the chain. Rather the path will have changed by the motion of other segments, *i.e.*, internal relaxation. What our result shows is that the effects of interior relaxation *average out* in the structure function as calculated within the reptation model. This also explains the observation in Section 4.2 that the discreteness of the individual steps is unimportant numerically. It yields only a correction to the second term in equation (4.20), which by itself is very small in the time range $\hat{t} \lesssim 10^3$, where discreteness corrections might show up. Deviations among theory and data which we will find for short times and wave vectors of the order of the inverse segment size therefore must originate from effects not taken into account in the reptation model.

In this context some further remark on the model of Rouse motion in a coiled tube seems appropriate. Concerning the *dynamics* along the tube, our hopping model is essentially equivalent to Rouse motion. Specifically, beyond microscopic times the motion of individual segments approaches Rouse-type motion, as has been shown in reference [16], Section 3. The difference found for the structure function results from the imposed initial conditions, only. It reflects the fact that the structure function measures correlations between two segments j , k and thus is influenced by the initial configuration of the subchain connecting j with k .

To summarize, we have seen that in the limit $N \rightarrow \infty$ with $q^2 R_g^2 \sim q^2 N$ kept fixed, the coherent structure function of the total chain varies only on scale T_3 . In this limit, $\bar{S}_c(q, t; N)$ is given by the primitive chain model. For shorter chains, tube length fluctuations come into play. They change the effective reptation time and lead to an initial decrease of \bar{S}_c on time scale T_2 . Both effects are important for chains up to lengths $N/N_e \approx 10^2$, at least. Proper internal relaxation, however, averages out.

With regard to the data presented in Section 5, we want to close this section with a brief discussion of the scattering $S_c(q, t; M, N)$ from the central subchain of length $M \ll N$ in a chain of finite length N . For small times (and sufficiently large wave vectors), we expect to see small fluctuations of the length of the part of the tube occupied by the subchain. Since, however, these fluctuations do not lead out of the original tube, they are much less efficient in reducing the scattering function than the tube length fluctuations relevant for the total chain: on average, up to times of the order of the relaxation time $T_2(M)$ of the subchain, its position in the tube has not changed seriously. A definite decrease of $S_c(q, t; M, N)$ sets in for times large enough for the subchain to leave its original part of the tube. For very large chain lengths N , this may occur for times $t \ll T_2(N)$. S_c then decreases like

$t^{-1/4}$, this law reflecting the $t^{1/4}$ -law (Eq. (1.1)) for the motion of an internal segment. For $T_2(N) \ll t \ll T_3(N)$, the motion of the subchain is driven by particles created by the chain ends which leads to a decrease like $t^{-1/2}$ (cf. Eq. (1.1)). Finally, of course, this behavior is cut off by tube destruction reaching the position of the subchain. On the quantitative level this behavior can be extracted from our theory. In the discussion of our data in some figures we will include curves which show the effect of relaxation of the (sub-) chain moving in an infinitely long tube, *i.e.*, neglecting all tube renewal effects.

4.4 Approximate analytical parameterization of our results for the total chain

The integral equations which yield the normalized coherent structure function $\bar{S}_c(q, t; N)$ of the full reptation model, can be solved only numerically. Furthermore, also the kernel and the inhomogeneity in these equations do not take a simple form [3]. In particular, the inhomogeneity is given by some integral with a lengthy integrand. Thus, to present the results in a more easily tractable form some more or less heuristic analytical parameterization might be useful.

It should be clear that such a parameterization cannot be very simple. The coherent scattering function involves two time scales: T_2 and T_3 . Furthermore, also wave vector and chain length combine into two relevant variables: $q^2 R_g^2$ and $q^2 \ell_0^2 \sqrt{N_e N} \sim q^2 R_g^2 \sqrt{N_e/N}$. The latter variable should govern the contribution of tube length fluctuations (cf. Eq. (4.15)). In searching for a reasonable parameterization, we exploit the fact that for very long chains our results reduce to those of the primitive chain model. Furthermore, as shown in Section 3.1, the functional form of \bar{S}_c , given by this model, can be used to fit the long-time tail also for non-asymptotic chain lengths. This suggests to use an ansatz similar to de Gennes' form (3.9):

$$\bar{S}_{\text{Fit}}(q, t; N) = (1-B)H(q, t; N) + B\bar{S}_{\text{DE}}\left(q^2 R_g^2, \frac{\hat{t}}{\hat{T}_{3,\text{Fit}}}\right). \quad (4.21)$$

The function $\bar{S}_{\text{DE}}(Q, \tau)$ is given by equations (3.2–3.5). Analyzing the numerical results of our theory in a large range of wave vectors and chain lengths which exceeds that used in the simulations, we find that the effective reptation time weakly depends on q . We use the expression

$$\hat{T}_{3,\text{Fit}} = \frac{3}{4} N_e^2 \left(\frac{N}{N_e}\right)^3 \cdot \left\{ 1 - \left[\frac{2.1}{(9+N/N_e)^{0.5}} - \frac{2.5}{9+N/N_e} \right] \cdot \left(1 + \frac{0.25}{(1+0.3q^2 R_g^2)^2} \right) \right\}. \quad (4.22)$$

The leading term gives the asymptotic law (4.12), the first correction is of order $\sqrt{N_e/N}$, in agreement with a result by Doi [6]. The prefactor of this correction differs somewhat from Doi's result. However, it must be noted that

equations (4.21–4.25) are meant to reproduce the scattering function in a wide parameter range. Thus, equation (4.22) should not literally be compared to Doi’s result.

We now turn to the coefficient B , which is taken as

$$B = \exp \left\{ - \left(\frac{q^2 R_g^2 \sqrt{\frac{N_e}{N}}}{1 + q^2 R_g^2 \sqrt{\frac{N_e}{N}}} \right)^{0.6} \frac{2.8}{2.4 + \sqrt{N/N_e}} \right\}. \quad (4.23)$$

This form is consistent with the discussion of the influence of tube length fluctuations given in the previous section. B tends to 1 for $q^2 R_g^2 \sqrt{N_e/N} \ll 1$ and yields $B \approx 1 - O(\sqrt{N_e/N})$ in the limit $N \rightarrow \infty$, q fixed.

The initial decrease of the scattering function over a sizeable range of time is approximated by a stretched exponential with an effective exponent which strongly decreases with increasing $q^2 R_g^2$. We take

$$H(q, t, N) = \exp \left\{ - \left(\frac{\hat{T}_2}{\hat{T}_{3,\text{Fit}}} \right)^{x_1} \left[3.2 \left(\frac{q^2 R_g^2}{0.7 + q^2 R_g^2} \right)^2 \frac{\hat{t}}{\hat{T}_2} \right]^{x_2} \right\}, \quad (4.24)$$

$$x_1 = 0.1 + \frac{0.9}{1 + 0.2q^2 R_g^2},$$

$$x_2 = 0.25 + \frac{0.75}{1 + 0.1q^2 R_g^2}. \quad (4.25)$$

We recall equation (4.9): $\hat{T}_2 = (N + 1)^2/\pi^2$.

The parameterization (4.21–4.25) is fitted to the numerical evaluation of our theory in the range $0.1 \leq q^2 R_g^2 \lesssim 50$; $10 \lesssim N/N_e \lesssim 340$; $0 \leq \hat{t} < \infty$. In most of that range it reproduces our full results within deviations less than 0.015 in absolute value. It becomes worse for shorter chains ($N/N_e \lesssim 30$) and larger wave vectors ($q\ell_0 \gtrsim 2$) in the large-time regime ($\hat{t} \gtrsim 0.1\hat{T}_3$). In this region the large-time tail predicted by the full theory deviates somewhat from the functional form given by the primitive chain model, and also small differences between the continuous and the discrete version of the model start to show up. For $N/N_e \lesssim 10$ our theory breaks down, mainly due to the fact that tube length fluctuations become important even for $\hat{t} \approx \hat{T}_3$. They thus affect the kernel $\mathcal{P}^*(j_0 t_0 | m)$ of the integral equation (4.2), and this effect has not been considered in our theory.

In the sequel we compare our Monte Carlo data to the results of the numerical evaluation of our full theory. It should be noted, however, that on the scale of the plots shown the difference between the results of the full theory and the effective parameterization (4.21–4.25) would be almost invisible.

5 Comparison of Monte Carlo data to full reptation theory

The reptation model in full detail treats the motion along the tube axis, but it does not account for all relaxation

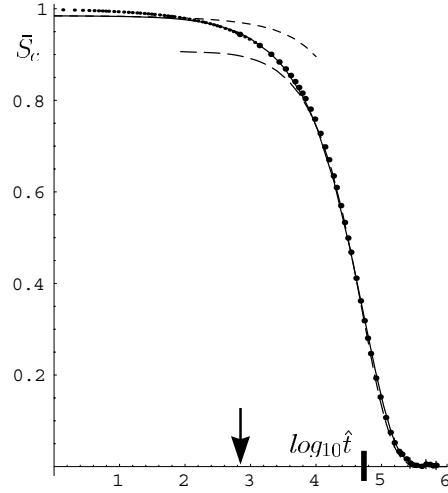


Fig. 7. Monte Carlo data for $\bar{S}_c(q, t, N)$ compared to reptation theory (full line), as function of $\log_{10} \hat{t}$. Chain length $N = 80$; wave vector $q = 0.5024$ ($q^2 R_g^2 = 3.32$). Long-dashed line: best fit to the primitive chain model (\bar{S}_{DE}). Short-dashed line: \bar{S}_c calculated neglecting tube destruction. The arrow points to \hat{T}_2 , the heavy slash gives \hat{T}_3 . Data, small dots: average over 10^4 short-time runs; heavy dots: averages over 50 medium-time runs.

processes in a realistic chain. In particular, motions “perpendicular to the tube”, like the creation and decay of larger side branches, will be present for the Monte Carlo chain but are not treated properly in the reptation model. Since larger side branches emerge by fusion of hairpins, they, in the framework of our model, would introduce some kind of interaction of the particles. Scattering vectors of magnitude $q \approx 1$ certainly resolve such effects which result in some additional relaxation on a microscopic time scale. In fitting the data to the theory we therefore allow for a phenomenological amplitude $A \leq 1$, multiplying the normalized structure function $\bar{S}_c(q, t; N)$ calculated for pure reptation. We typically find values $A \approx 0.9$ for $q = 1$, $A \approx 0.98$ for $q = 0.5$, and $A \approx 1$ for all smaller q measured. Thus, the deviations among theory and data which are found for small times, rapidly decrease with decreasing q .

For a first illustration, in Figure 7 we show our results for $N = 80$, $q = 0.5024$ ($q^2 R_g^2 = 3.32$). Data points result from runs extending to 10^5 or 10^8 Monte Carlo steps. The full curve gives the result of our theory, with the amplitude adjusted to $A = 0.985$. Long dashes represent a fit to the primitive chain model, with B_{DE} and $\hat{T}_3 = \tau_0 T_3^{(\text{MC})}$ taken from Table 1. The short-dashed curve results by neglecting tube destruction and is calculated as the structure function of a chain of length N in an infinitely long tube. Since the primitive chain model takes care only of tube destruction, the difference among the two dashed curves is due to tube length fluctuations. Thus Figure 7 demonstrates that the tube length fluctuations strongly influence the structure function up to times $t \approx T_2$. For much larger-times tube destruction is the dominant process.

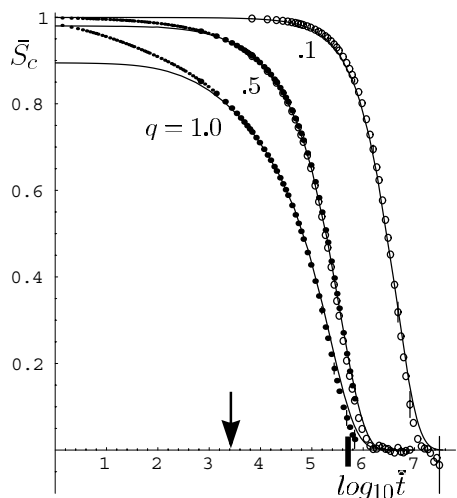


Fig. 8. Data compared to reptation theory. $N = 160$; $q = 0.1$ ($q^2 R_g^2 = 0.267$); $q = 0.5$ ($q^2 R_g^2 = 6.665$); $q = 1.0$ ($q^2 R_g^2 = 26.61$). Arrow: \hat{T}_2 ; slash: \hat{T}_3 . Small dots: short-time runs; heavy dots: runs for intermediate time; circles: long-time runs. The time regimes overlap. Some error bars (two standard deviations) are also given.

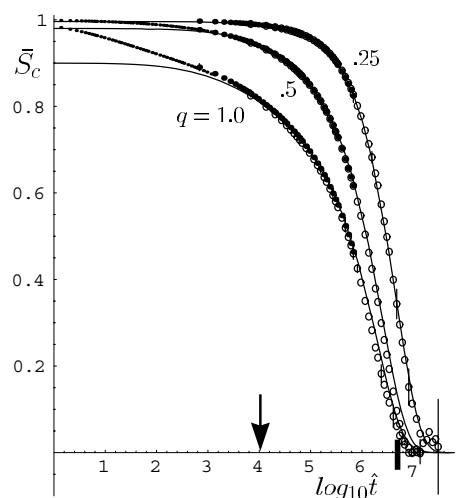


Fig. 9. Same as Figure 8, but for $N = 320$; $q = 0.25$ ($q^2 R_g^2 = 3.33$); $q = 0.5$ ($q^2 R_g^2 = 13.33$); $q = 1.0$ ($q^2 R_g^2 = 53.22$).

These results are typical for all chain lengths and wave vectors. Figures 8 and 9 show our results for $N = 160$ and 320, respectively. Beyond some short-time regime, we find excellent agreement between theory and data, with only the amplitude $A = A(q, N)$ taken as adjustable parameter. Comparing Figure 9 to Figure 4, (note the difference of time scales: $\log_{10} \hat{t} = \log_{10} t^{(MC)} - 1.167$), we again see the effect of tube length fluctuations: for $N = 320$, the primitive chain model can fit the data only for $t \gtrsim 20T_2$. For smaller times, tube length fluctuations become relevant, their effect increasing with increasing q , as expected. For $N = 160$, $q = 0.1$ ($q^2 R_g^2 \approx 0.267$), scattering cannot resolve the structure of the tube and the effect of tube

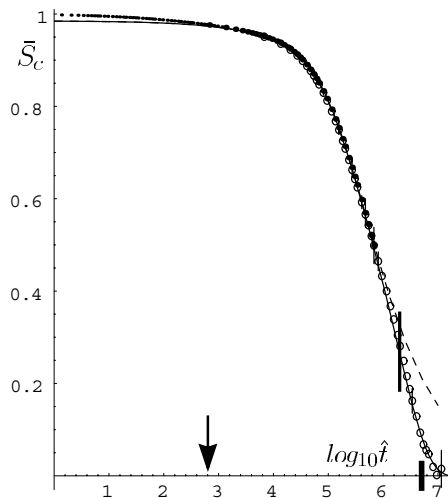


Fig. 10. Coherent structure function of the central piece of length $M = 80$ in a chain of length $N = 320$, normalized to the static structure function of a chain of length M . Wave vector $q = 0.5$. Full line: full result of the theory; broken line: result neglecting tube destruction. The long slash through the curve at $\log_{10} \hat{t} \approx 6.27$ gives the time where tube destruction on average reaches the subchain $M = 80$, as derived from our theory. Other symbols as in Figures 8 and 9.

length fluctuations is suppressed. The corresponding curve shown in Figure 8 essentially coincides with the result of the primitive chain model, provided we adjust the effective time scale T_3 .

To gain additional information on the chain dynamics, we also measured and calculated the structure function of the central piece of length M in a chain of length N . Figure 10 shows our results for $M = 80$, $N = 320$, $q = 0.5$. With these parameter values it is directly comparable to Figure 7, where $M = N = 80$, $q = 0.5024$. The central piece evidently is not influenced by tube length fluctuations. In contrast to Figure 7, the decrease of $\bar{S}_c(q, t; M, N)$, in Figure 10 must be due to relaxation within the initial tube, up to times where tube destruction reaches the subchain measured. Indeed, in Figure 10 the structure function calculated neglecting tube destruction (broken line) over a large time range coincides with the results of our full theory and simulations. The time $T_R(M, N)$ it needs for tube destruction to reach the subchain, can be estimated from the relation

$$\bar{\ell}_{Sn_{\max}}(T_R(M, N)) = \frac{1}{2}(N - M). \quad (5.1)$$

This time is indicated in Figure 10 and is close to the time where the dashed line starts to deviate from our full result. Recall from Section 4.1 that $\bar{\ell}_{Sn_{\max}}(t)$ gives the average length of the end-piece of the tube that has been destroyed up to time t .

As pointed out in Section 4.3, the decrease of $\bar{S}_c(q, t; M, N)$ seen in Figure 10 in the range $t < T_R(M, N)$ is not due to relaxation within the subchain M considered, but results from the internal dynamics of the total

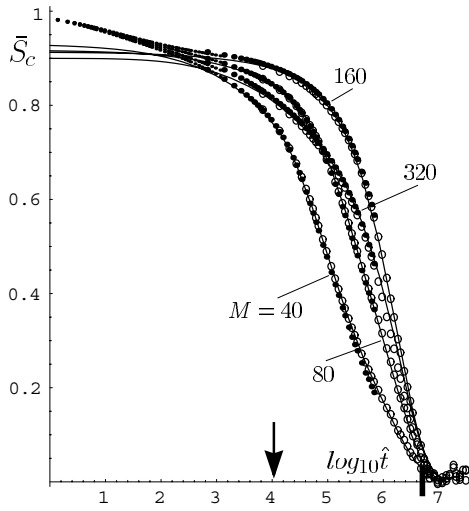


Fig. 11. Normalized coherent structure functions of central subchains of lengths M in a chain of length $N = 320$. Wave vector $q = 1.0$. $M = 320$ represents scattering from the total chain. Symbols are as in Figures 8, 9.

chain which leads to fluctuations of the position of the subchain in the original tube. This is illustrated in Figure 11, which for given $N = 320$ and $q = 1.0$ compares the scattering from central subchains of lengths $M = 40, 80, 160, 320$. We note some peculiar behavior: as function of time, the normalized scattering function of the total chain $M = N = 320$ initially decreases faster and eventually crosses results for internal pieces. This shows the efficiency of tube length fluctuations in comparison to the internal dynamics of the chain. According to the discussion of Section 4.3, subchains $M \lesssim N - \sqrt{\frac{1}{3}N_e N} \approx 300$ (for $N = 320$) are not influenced by tube length fluctuations, and for a large time range scattering from such subchains is determined by the diffusive motion of the total subchain in the initial tube. Since the diffusion coefficient of this motion scales as $1/M$, the diffusion of the longer subchains is very slow. Taking place in the initial tube, it is also less efficient in reducing \bar{S}_c than tube length fluctuations or the tube destructing shift of the total chain. For these reasons, the normalized coherent scattering for $M = 160$ stays above the result for the total chain up to times $t \approx T_3(N)$. For larger times the theory predicts that as for the shorter subchains the normalized scattering from subchain $M = 160$ falls below the scattering from the total chain, but the effect is too small to be visible in Figure 11, and it is clearly not resolved by the accuracy of the data. We also note that tube destruction reaches the initial position of the subchain $M = 160$ only for $pT_R(160, 320) \approx 10^{5.8}$. With decreasing M , diffusion in the tube becomes faster, and for the shortest subchain, $M = 40$, we see indications of a new regime: the slope of the curve seems to change near $\hat{t} = 10^{5.4}$. A doubly logarithmic plot reveals that in the range $10^{5.4} \leq \hat{t} \leq 10^{6.1}$ the data approach a $\hat{t}^{-1/2}$ -law, and the upper bound of this interval is close to the time $pT_R(40, 320) \approx 10^{6.4}$.

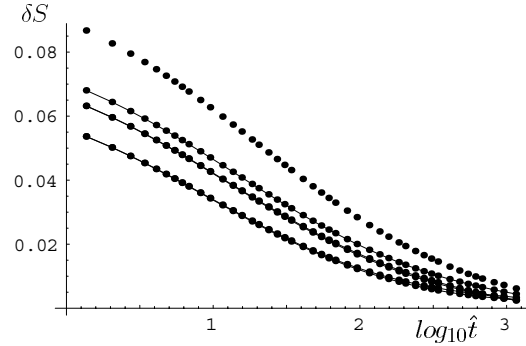


Fig. 12. Deviation between theory and experiment: $\delta S = \bar{S}$ (Monte Carlo) $- A \cdot \bar{S}$ (theory), for $q = 1.0$. Connected data points: results for $M = 40$ ($N = 160, 320$), $M = 80$ ($N = 160, 320$), $M = 160$ ($N = 320$) (from below). For $M = 40, 80$ the results for the two different lengths N of the total chain fall right on top of each other. Disconnected points: $M = N = 160$.

These observations are consistent with the discussion of Section 4.3.

Finally, we consider the deviations between theory and data present for $\hat{t} \lesssim 10^3$ and large wave vectors. A first important observation is that these deviations roughly are of the same size for interior pieces of the chain as for the total chain, see Figure 11. Therefore, their dominant source cannot be searched in our treatment of tube length fluctuations in the mean hopping rate approximation. To show this in more detail, in Figure 12 we have plotted the deviation between data and theory for wave vector $q = 1.0$ and all chains and subchains measured. We note some end-effect: for the total chain $N = 160 = M$ the deviation is about 20% larger than for the central piece $M = 160$ in the chain $N = 320$. However, the bulk of the effect is independent of $N > M$, as illustrated by the curves for $M = 40$ and $M = 80$, which each in fact combine data for $N = 160$ and $N = 320$. For these internal pieces, tube length fluctuations are irrelevant, and in the time range shown, our evaluation of the reptation model is exact within the accuracy (0.5%) of our numerics. Consequently, the initial deviations must be dominated by some relaxation in the interior of the subchain M which is not taken into account by the reptation model. We note that the amplitude A of the effect depends on M only weakly, but strongly increases with q , as is illustrated by Figures 8 and 9. It is roughly proportional to q^2 . These observations are consistent with an interpretation as micro-structure effects, which clearly increase strongly with the resolving power of the experiment and are expected to show a weak dependence $\sim 1/M$ on (sub-)chain length.

In our previous work on the motion of individual segments, we found initial transients which also decayed on a time scale $\hat{t} \lesssim 10^3$. These could be traced back to the discreteness of both the hopping process and the underlying chain and could be largely explained by a fully discrete analysis of our model. As mentioned in Section 4.1, it turns out that for $\bar{S}_c(q, t, M, N)$ this discreteness numerically is irrelevant. In the light of the discussion of Section 4.3,

this is quite understandable: the internal dynamics of the subchain averages out. We thus have to search for effects going beyond our implementation of the reptation model. One source of discrepancy immediately comes into mind. A particle sitting on a bead is not an exact representation of a hairpin. It is not clear, for instance, whether the bead sits in the tip or in the base of the hairpin. Simple estimates of such effects easily yield a correction amplitude $1 - A$ of the desired order of magnitude. However, the dynamics of single hairpins cannot explain a time scale of order 10^3 since it relaxes essentially within one Monte Carlo step. Slower relaxation occurs for larger side branches. Already a structure created by fusion of two hairpins shows a relaxation time of the order of 10 MC steps. Indeed, the fusion of hairpins destroys mobile units of the Monte Carlo chain. In the language of our model this induces some dynamical interaction of the particles. We, therefore, believe that the observed initial transients are due to the interference of reptation with the dynamics of larger side branches.

6 Conclusions

In this paper, we presented results of simulations of the Evans-Edwards model, measuring the coherent structure function of a reptating chain in a large range of time and wave vector. This model contains the full reptational dynamics of a single chain, including internal relaxation, tube length fluctuations, and tube renewal, but omits all the dynamics of the environment. In particular, it ignores constraint release. We compared the data to two simplified versions of the reptation model as well as to our recent evaluation of the full theory. We found that the primitive chain model proposed by Doi and Edwards [4,2] yields a good fit to the data for times large compared to the Rouse time T_2 , provided we allow for a phenomenological amplitude factor and treat the reptation time T_3 as a second adjustable parameter. De Gennes' approach [5] which adds a contribution meant to take one-dimensional internal relaxation along the tube into account, cannot explain the data consistently. So the success of this approach in fitting neutron scattering data on polymer melts [21–23] indicates that the local contribution $S^{(\ell)}(q, t)$ to De Gennes' structure function phenomenologically accounts for some dynamics not contained in the reptation model. In view of our findings for the Evans-Edwards model we would search the origin of the observed initial decay in a coupling of reptation to motion perpendicular to the tube. Since in the experimental time range the initial decay accounts for most of the variation of the experimental curves [23], we have not tried to fit these curves with our theory.

Provided we allow for a single adjustable amplitude factor we find, beyond the short time range influenced by microstructure relaxation, quantitative agreement between our simulation data and our analytical evaluation [3] of full reptation theory. The theory in all details explains not only the scattering function of the total chain but also the scattering from interior subchains. Except

for the phenomenological amplitude, which notably differs from 1 only for wave vectors of the order of the inverse segment size, all parameters of the theory are essentially fixed by our previous analysis [16,17] of the motion of internal segments. Thus, our version of the reptation model consistently explains both details of the internal motion and global features like the scattering function.

Our analysis shows that the effects of internal relaxation contained in the reptation model and seen, for instance, in the motion of internal segments, for the scattering functions average out. In the reptation model, the time dependence of the scattering functions is determined solely by the interplay of tube destruction and tube length fluctuations. The latter not only determine the scattering function up to times of order T_2 , but also for intermediate chain lengths lead to the decrease [6] of the reptation time T_3 in comparison to the asymptotic law, clearly seen also in the scattering function. Numerically evaluating our theory, we found these effects to be well visible up to chain lengths of the order of 300 entanglement lengths. This is obvious from the numerical parameterization of our results, given in Section 4.4.

Our theory deviates from the results of the simulation in the initial time region $t \lesssim 10^3$. We stress that this is not due to the approximations inherent in our treatment of tube destruction. Deviations of the same order of magnitude occur for the total chain and for internal subchains, and the coherent structure function of internal subchains in the initial time region is not affected by our approximations. Thus, the need to introduce some phenomenological parameter to take short time relaxation into account illustrates that even for the Evans-Edwards model, which is the most accurate computer-experimental implementation of the reptation model we can think of, some relaxation “perpendicular” to the tube shows up. Clearly, for a melt, such effects must be much larger. However, our analysis suggests some way to suppress these contributions. The scattering from a chain of length $N = M$ should be compared to the scattering from the central piece of length M in a chain of length $N \approx 2M$. Up to small end-effects, the difference of the two coherent scattering functions should be due to reptation alone, and can be calculated from our theory. To observe an effect, the experiments must cover a time range extending at least up to the Rouse time, with chain length being of the order $N/N_e \gtrsim 20$. Unfortunately, for physical experiments, this seems to be out of reach. As shown by the work of reference [10] it might be feasible in simulations.

This work was supported by the Deutsche Forschungsgemeinschaft, SFB 237.

References

1. P.G. De Gennes, *J. Chem. Phys.* **55**, 572 (1971).
2. M. Doi, S.F. Edwards, *The Theory of Polymer Dynamics* (Clarendon Press, Oxford, 1986).
3. L. Schäfer, U. Ebert, A. Baumgärtner, *Phys. Rev. E.* **65**, 061505 (2002).

4. M. Doi, S.F. Edwards, J. Chem. Soc. Faraday Trans. 2, **74**, 1789 (1978).
5. P.G. de Gennes, J. Phys. (Paris) **42**, 735 (1981).
6. M. Doi, J. Polymer Sci. Polymer Phys. Ed. **21**, 667 (1983).
7. T.P. Lodge, N.A. Rotstein, S. Prager, in *Advances in Chemical Physics LXXIX*, edited by Prigogine and Rice (Wiley, 1990).
8. P.G. De Gennes, J. Phys. (Paris) **36**, 1199 (1975).
9. T. Kreer, J. Baschnagel, M. Müller, K. Binder, Macromolecules **34**, 1105 (2001).
10. M. Pütz, K. Kremer, G.S. Grest, Europhys. Lett. **49**, 735 (2000).
11. R. Graf, A. Heuer, H.W. Spiess, Phys. Rev. Lett. **80**, 5738 (1998).
12. R. Kimmich, R.-O. Seitter, U. Beginn, M. Möller, N. Fatkullin, Chem. Phys. Lett. **307**, 147 (1999).
13. W. Hess, Macromolecules **19**, 1395 (1986).
14. K.S. Schweizer, M. Fuchs, G. Szamel, M. Guenza, H. Tang, Macromol. Theory Simul. **6**, 1037 (1997).
15. U. Ebert, A. Baumgärtner, L. Schäfer, Phys. Rev. Lett. **78**, 1592 (1997).
16. U. Ebert, L. Schäfer, A. Baumgärtner, J. Stat. Phys. **90**, 1325 (1998).
17. A. Baumgärtner, U. Ebert, L. Schäfer, J. Stat. Phys. **90**, 1375 (1998).
18. K.E. Evans, S.F. Edwards, J. Chem. Soc., Faraday Trans. 2, **77**, 1891 (1981).
19. L. Schäfer, A. Baumgärtner, U. Ebert, Eur. Phys. J. B **10**, 105 (1999).
20. R.D. Willmann, J. Chem. Phys. **116**, 2688 (2002).
21. P. Schleger, B. Farago, C. Lartigue, A. Kollmar, D. Richter, Phys. Rev. Lett. **81**, 124 (1998).
22. A. Wischnewski, D. Richter, Europhys. Lett. **52**, 719 (2000).
23. A. Wischnewski, M. Monkenbusch, L. Willner, D. Richter, A.E. Likhtman, T.C.B. McLeish, B. Farago, Phys. Rev. Lett. **88**, 058301 (2002).
24. M. Pütz, K. Kremer, G.S. Grest, Europhys. Lett. **52**, 721 (2000).
25. F. Spitzer, *Principles of Random Walk* (Springer, Heidelberg, 1976).